CrossMark

Potential impact of the Pacific Decadal Oscillation and sea surface temperature in the tropical Indian Ocean–Western Pacific on the variability of typhoon landfall on the China coast

Lei Yang[1] · Sheng Chen[1] · Chunzai Wang[1] · Dongxiao Wang[1] · Xin Wang[1,2]

Abstract

The landfall activity of typhoons (TYs) along the coast of China during July–August–September (JAS) shows significant interdecadal variation during 1965–2010. We identify three sub-periods of TY landfall activity in JAS along the China coast in this period, with more TY landfall during 1965–1978 (Period I) and 1998–2010 (Period III), and less during 1982–1995 (Period II). We find that the interdecadal variation might be related to the combined effects of Pacific Decadal Oscillation (PDO) phase changes and sea surface temperature (SST) variation in the tropical Indian Ocean and Western Pacific (IO–WP). During the negative PDO phase in Periods I and III, a cyclonic anomaly is located in the western North Pacific (WNP), inducing easterly flow in its northern part, which favors TY landfall along the eastern China coast. Warm SST anomalies over the tropical IO–WP during Period III induce an anomalous anticyclonic circulation in the WNP through both the Gill-pattern response to the warm SST in the tropical IO and the anomalous meridional circulation induced by the warm SST in the tropical WNP. As a result, the northern South China Sea and WNP (10°–20° N) are dominated by southeasterly flow, which favors TYs making landfall on both the southern and eastern China coast. With both landfalling-favorable conditions satisfied, there are significantly more TYs making landfall along the China coast during Period III than during Period I, which shows cool SST anomalies in the tropical IO–WP.

1 Introduction

Tropical cyclones (TCs) that make landfall can cause severe economic losses in coastal regions. TC track direction is one of the major factors that should be included in TC landfall prediction (Wang and Chan 2002; Liu and Chan 2003; Yang et al. 2015a, b). Previous studies have shown that the interannual and interdecadal variability of TC activity in the western North Pacific (WNP) is closely related to the El Niño–Southern Oscillation (ENSO), Pacific Decadal Oscillation (PDO) and East Asian monsoon variability (Wang et al. 2012; Yuan et al. 2014). As the most important mode in

the topical air–sea interaction, ENSO has a strong influence on the interannual variability of TC activity (Saunders et al. 2000; Sobel and Maloney 2000; Wang and Chan 2002; Wu et al. 2005; Camargo and Sobel 2005; Chan 2006; Zhang et al. 2012a, b; Wang and Wang 2013; Wang et al. 2014; Kim et al. 2016). A previous study found that the interannual variation of TC tracks and landfall along the South China coast is strongly influenced by ENSO events (Liu and Chan 2003). The study found fewer (more) TCs making landfall along the southern China coast during strong El Niño (La Niña) events, especially during the late TC season (October–November), which is attributable to an eastward (westward) shift of the TC genesis location. During early summer (May–June) after La Niña (El Niño) years, there are more (fewer) TCs making landfall along the southern China coast, due to the existence of a persistent low-level cyclone (anticyclone) over the Philippines. Huang and Wang (2010) found that the interannual variability of TC landfall along the eastern and southern coast of China is positively correlated with the summer East Asia–Pacific index during 1979–2007. They found that more TCs making landfall along the coast north (south) of Xiamen corresponds to a

✉ Xin Wang
wangxin@scsio.ac.cn

1 State Key Laboratory of Tropical Oceanography (LTO), South China Sea Institute of Oceanology, Chinese Academy of Sciences, 164 West Xingang Road, Guangzhou 510301, China

2 Laboratory for Regional Oceanography and Numerical Modeling, Qingdao National Laboratory for Marine Science and Technology, Qingdao 266237, China

positive (negative) East Asia–Pacific index, indicating a northeastward (southwestward) shift of the Western Pacific subtropical high (WPSH), which leads to TCs moving northward (southward) and making landfall along the east (south) coast of China. They also found that TCs making landfall along the east (south) coast of China show an increasing (decreasing) trend. Using a regional climate model, Jin et al. (2013) confirmed that more instances of typhoon (TY) landfall in the East Asian coastal region during July–October are mainly related to the northern off-equatorial central Pacific sea surface temperature (SST) warming, which induces anomalous easterly steering flows that direct more WNP TCs towards the East Asian coastline.

The PDO can influence the track pattern of WNP TCs by regulating the large-scale atmospheric circulation (Chan and Zhou 2005; Zhou et al. 2007; Liu and Chan 2008; Li et al. 2017). The interdecadal variability of TC landfall in the Philippines has been found to be related to the PDO and ENSO (Kubota and Chan 2009). There are several studies that have discussed the interdecadal variability of WNP TC track patterns and their landfall characteristics during different time periods. From 1951–1979 to 1980–2001, TC passage in the South China Sea (SCS) increased slightly, while it decreased in the eastern China Sea and the Philippine Sea (Ho et al. 2004). Wu et al. (2005) found that TCs making landfall along the east (south) coast increased (decreased) during 1965–2003 due to a westward shift of prevailing TC (June–October) tracks in the WNP. By investigating the WNP TC activity during the entire year instead of only summer, Liu and Chan (2008) identified four sub-periods in terms of the TC occurrence pattern in the WNP during 1960–2005. The variations in the TC occurrence pattern led to more (fewer) TCs making landfall along the South China coast during 1964–1976, 1977–1988 and 1989–1997 (1998–2005), and more (fewer) along the East China coast during 1977–1988 and 1998–2005 (1964–1976 and 1989–1997). This interdecadal variability may be partly related to the PDO (Liu and Chan 2008).

In this study, we first identify three periods during 1965–2010 according to the typhoon landfall activity along the China coast: (I) high (1965–1978); (II) low (1982–1995); and (III) higher (1998–2010). We then further explore the underlying mechanisms. The higher TC landfall activity during Period III is found to be closely related to both the PDO phase and the SST anomalies over the tropical Indian Ocean and Western Pacific (IO–WP).

2 Datasets and models

To examine TC landfall along the China coast, data on TCs that formed in the WNP during 1965–2010 are obtained from the International Best Track Archive for Climate Stewardship (IBTrACS) dataset (V03r09; Knapp et al. 2010). The dataset includes six-hourly TC center locations from 12 different agencies and historical databases from 1884 to 2015. Data before 1965 are not considered in this study due to their possible low reliability during that time (Wu et al. 2005). As large uncertainty might exist in the landfall records of weaker TCs, we only consider TCs with a maximum surface wind speed of 32.4 m s^{-1} or higher [i.e., typhoon (TY)]. In this study, we investigate the TY activity that occurs during July–September (JAS), which is the main TC season in the WNP.

Monthly geopotential height and horizontal wind data at standard pressure levels are obtained from the National Centers for Environmental Prediction (NCEP) reanalysis (Kalnay et al. 1996). The horizontal resolution of these data is $2.5° \times 2.5°$. The Met Office's Hadley Centre Sea Ice and Sea Surface Temperature (HadISST) dataset (Rayner et al. 2003; Kennedy et al. 2011) is used to analyze the tropical IO–WP SST variation and its relationship to large-scale atmospheric circulations.

Steering flows, which represent the large-scale circulation that directs TC motion (e.g., Holland 1983), are calculated by integrating the pressure-weighted layer flows between two atmospheric layers (Chan and Gray 1982; Dong and Neumann 1986; Chu et al. 2012). Wind data are integrated at grid points from 850 to 200 hPa. Anomaly fields are obtained by subtracting a long-term monthly climatology (average during 1965–2010) from the original monthly data. The PDO index was obtained from http://www.esrl.noaa.gov/psd/data/climateindices/list.

To further confirm the potential influence of tropical IO–WP SSTs and the PDO on the interdecadal variability of steering flow, several numerical experiments are conducted with version 5.0 of the National Center for Atmospheric Research (NCAR) Community Atmospheric Model (CAM5), which has a horizontal resolution of $3.75° \times 3.75°$ and 30 vertical levels. CAM is the atmospheric component of the NCAR Earth System Model. Considerable improvements in the boundary layer condition and shallow cumulus scheme have been made in this version (Bretherton and Park 2009; Neale et al. 2010). In this study, we use the HadISST dataset as the lower boundary conditions to drive all model runs.

3 Interdecadal variation of TY landfall along the China coast

The number of WNP TYs making landfall on the China coast during 1965–2010 shows strong interannual and interdecadal variability (Fig. 1). To exclude the influence of genesis number on the landfall variability, we also calculate the percentage of generated WNP TYs that made landfall,
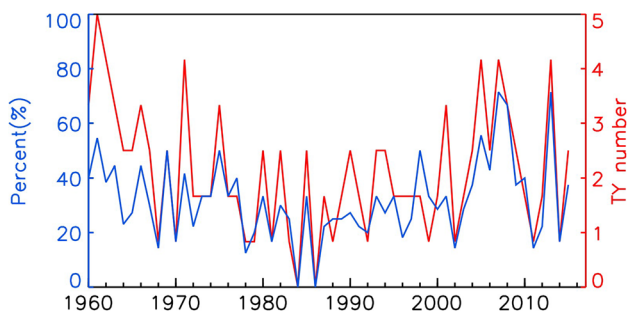
Fig. 1 Time series of JAS TY landfall number (red) and the TY landfall percentage of the total TY numbers in the WNP (blue) on the China coast during 1960–2015
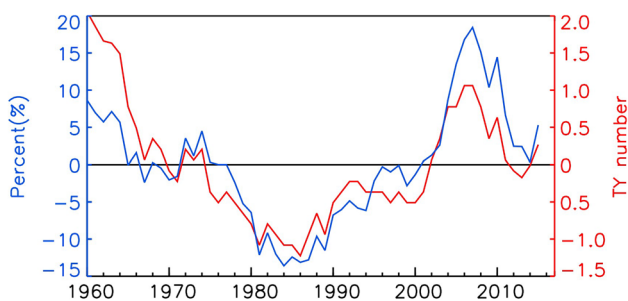

Fig. 2 Time series of the anomalies of the 7-year running mean of JAS TY landfall number (red) and the TY landfall percentage of total TY numbers in the WNP (blue) on the China coast during 1960–2015

which shows similar variability to the landfall number (Fig. 1). Based on the 7-year running mean of TY landfall number and percentage, three phases of TY landfall activity are identified (Fig. 2): (I) high (1965–late 1970s); (II) low (early 1980–mid-1990s); and (III) higher (late 1990s–2015). To further examine the underlying mechanism, we define the three periods as: (I) high (1965–1978); (II) low (1982–1995) and (III) higher (1998–2010). Period III does not include 2011–2015 because of a possible phase change of the PDO after 2010.

The mean value of TY landfall on the China coast for 1965–1978, 1982–1995, and 1998–2010 is 1.7, 0.8 and 2, respectively (Table 1). The difference in the mean values of TY landfall number between the high landfall activity

periods (I and III) and the low landfall activity period is statistically significant at the > 95% confidence level. Therefore, the first question we aim to answer in this study is: What are the physical mechanisms for the higher or lower TY landfall activity on the China coast? It is also noted that both the TY landfall number and percentage during Period III are significantly higher than during Period I. Whether there is an additional controlling factor during Period III (1998–2010) is the second question this study aims to answer. In the following, we explore the main mechanisms for the low and high landfall activity along the China coast.

The overall pattern of the average steering flow during Periods I and II is similar, showing a westerly steering flow from East Asia to the northern WNP (Fig. 3a, b). The difference between Periods I and II (Period I minus Period II) shows an anomalous easterly–northeasterly flow over the northern WNP (but does not exceed the 95% significance level) and southwesterly flow over South Asia (exceeds the 95% significance level). The two flows converge and turn northeastward along the southern and eastern China coast (Fig. 3c), which favors westward TC tracks and landfall on the China coast. TY genesis occurrence (grouped into a 1×1 grid) is also added in Fig. 3 to show both the number and their distribution of TY generated in the WNP (Fig. 3a–c). Relatively more TYs are generated in the WNP east of the Philippines during Period I (negative PDO phase) (Fig. 3b), while more TYs are generated farther east in the WNP during Period II (positive PDO phase) (Fig. 3a). A higher TY genesis number east of Philippines during the negative PDO phase might be due to the positive vorticity in that area (Goh and Chan 2009). There is a higher possibility for these TYs to enter the area that is dominated by anomalous easterly steering flow, and move westward making landfall on the China coast. In fact, Goh and Chan (2009) noticed that more WNP TCs enter SCS during negative PDO phases, and more recurved TCs during positive PDO phases.

By looking at the 500 hPa geopotential height, it is found that a large anticyclonic circulation is located over the WNP in both Periods I and II (Fig. 4a, b). The anticyclonic circulation during Period II extends more westward than that during Period I, which is in agreement with earlier studies (e.g., Zhou et al. 2009). As a result, the difference between Periods I and II (Period I minus Period II) exhibits a significant

Table 1 The impact of PDO phase and tropical IO–WP SST anomalies on the TY landfall numbers (↑ represents positive impact and ↓ represents negative impact) and mean TY landfall number for the three periods

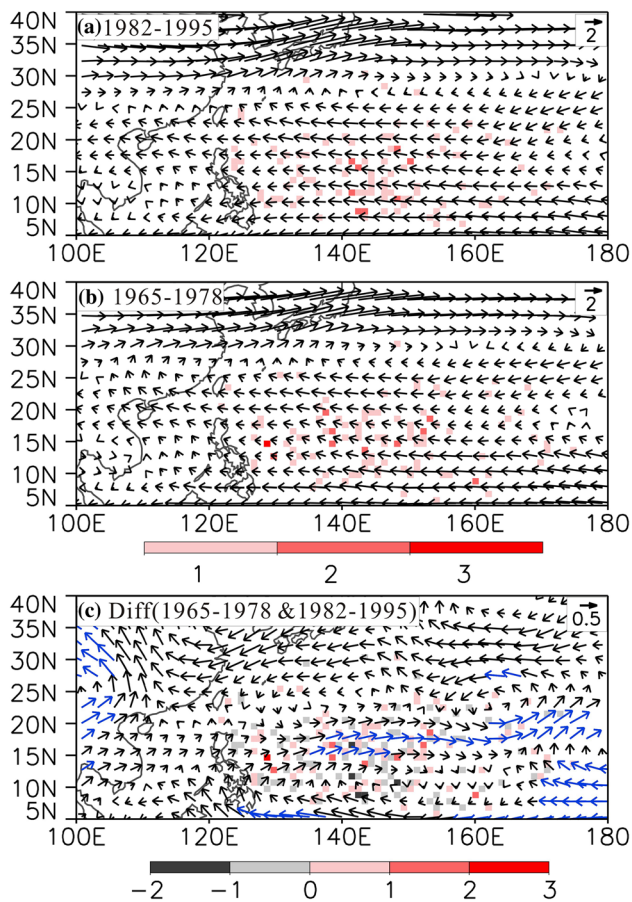| Period	1965–1978		1982–1995		1998–2010	
PDO/IO–WP phase	PDO (−)	IO–WP (−)	PDO (+)	IO–WP (+)	PDO (−)	IO–WP (+)
Impacts on TY landfall at China coast	↑	↓	↓	↑	↑	↑
Mean TY landfall	1.7		0.8		2	

Fig. 3 Average steering flow during **a** Period II and **b** Period I, and **c** the difference (**b** minus **a**). Red shading in **a** and **b** represents the occurrence (1×1 grid) of TY genesis in the WNP. Red and gray shading in **c** represents the differences (**b** minus **a**). Blue vectors in **c** exceed the 95% significance level

Fig. 4 Average 500 hPa geopotential height during **a** Period II and **b** Period I, and **c** the difference (**b** minus **a**). Gray lines in **a** and **b** represent the WNP TY tracks that make landfall on the China coast. Red dots in **c** indicate those exceeding the 95% significance level

cyclonic circulation over the WNP (Fig. 4c), which favors anomalous easterly flow, as shown in Fig. 3c. The influence of the WPSH on the WNP TC activity and the East Asian summer monsoon varies with its shape, position and intensity (Chan and Xu 2009; Wang et al. 2013; Feng and Hu 2014). Zhou et al. (2009) related the westward extension of the WPSH to IO–Maritime Continent (MC) warming using numerical experiments. They found that warming in the IO–MC region influences the Walker circulation and results in negative heating in the central and eastern Pacific, which then triggers anomalous anticyclones in the Pacific through an ENSO–Gill-type response.

Similar to the difference in steering flow between Periods I and II, the difference between Periods III and II also shows an easterly anomaly north of 20°N, but is much stronger and persistent from the northern WNP to East Asia (Fig. 5a–c). Compared with Period II (Fig. 5a), more WNP TYs are generated east of the Philippines (Fig. 5b) during Period III. The difference in TY genesis location is similar to that between
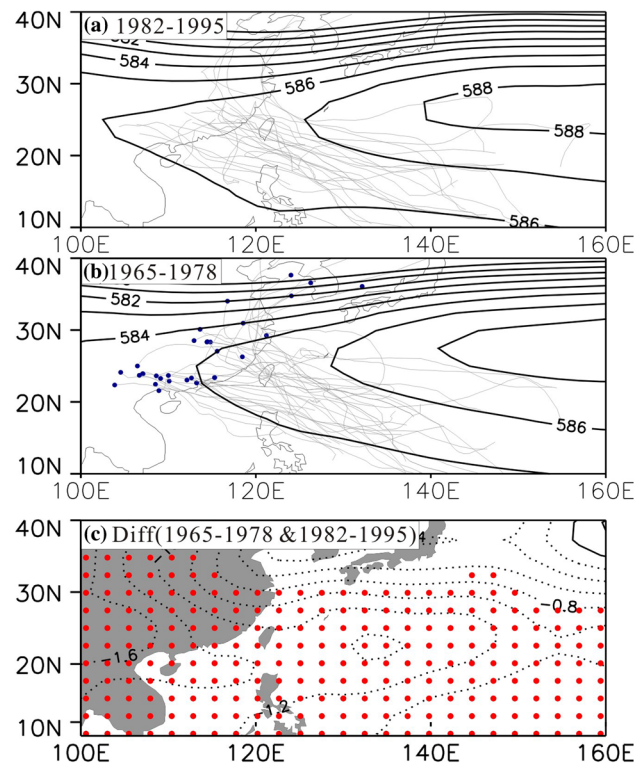
Periods I and II (Fig. 5c), due to the different response to the different PDO phases, which is consistent with previous studies (e.g., Goh and Chan 2009). When we further compare the TY genesis location between the two negative PDO phases, we find that the high number of WNP TYs generated east of the Philippines area is more obvious during Period III than during Period I. The difference might be related to the positive vorticity anomaly resulting from the warm IO–WP SST during Period III (Fig. 5d). It is more likely that WNP TYs generated east of the Philippines are controlled by the strong steering flow anomaly northwest of the TY genesis area, which increases the possibility of TYs making landfall on the China coast.

By comparing the 500 hPa geopotential height during Periods II and III, it is found that the WPSH extends farther westward during Period III (Fig. 6a, b). The difference in 500 hPa geopotential height between Periods II and III (Period III minus Period II) exhibits cyclonic circulation over the WNP (Fig. 6c). Another cyclonic center is present over southern Asia, further strengthening the eastward flow anomalies (Fig. 6c).

Although the WPSH extends westward from Period I to Period III, the pattern varies between years. As shown above, the difference in the 500 hPa geopotential height
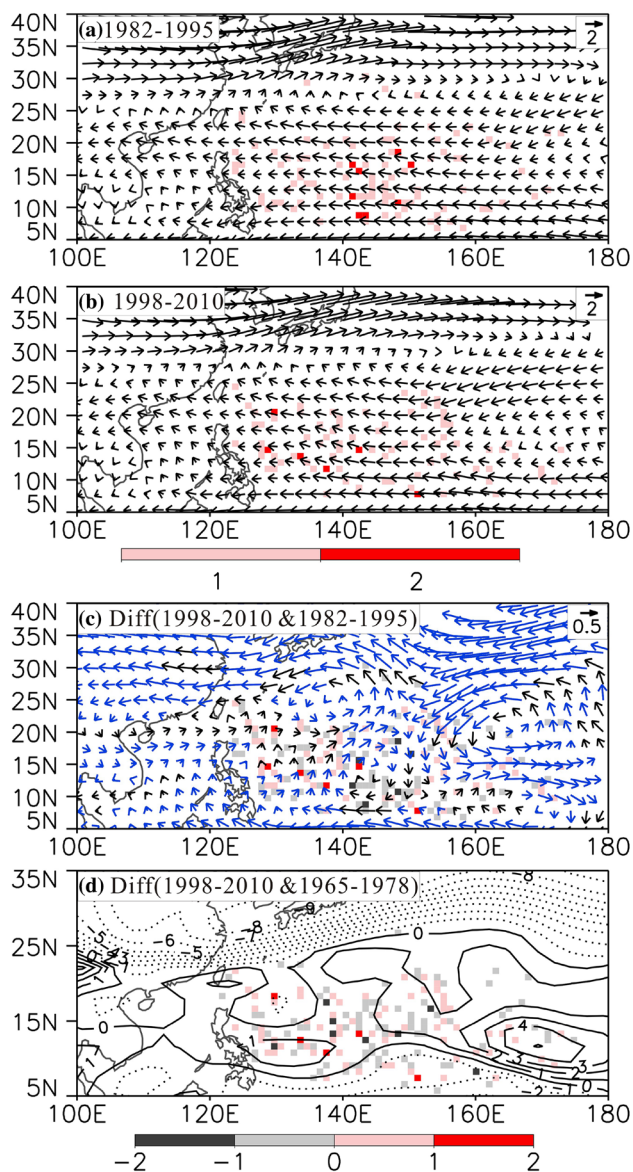
Fig. 5 Average steering flow during **a** Period II and **b** Period III, and **c** the difference (**b** minus **a**). Red shading in **a** and **b** represents the occurrence (1×1 grid) of TY genesis in the WNP. Red and gray shading in **c** represents the difference (b minus a). Blue vectors in **c** exceed the 95% significance level. **d** Difference in 850 hPa relative vorticity ($\times 10^{-6}$ s^{-1}) between Periods III and I. Red and gray shading in **c** represents the difference in TY genesis number between Periods III and I (Period III minus Period I)

Fig. 6 Average 500 hPa geopotential height during **a** Period II and **b** Period III, and **c** the difference (**b** minus **a**). Gray lines in **a** and **b** represent the WNP TY tracks that make landfall on the China coast. Red dots in **c** indicate those exceeding the 95% significance level

Fig. 7 Difference in average geopotential height (contours) and wind (vectors) at 500 hPa: **a** Period II (1982–1995) minus Period I (1965–1978) and **b** Period III (1998–2010) minus Period II (1982–1995)

between Periods II and III (Period III minus Period II) exhibits a cyclonic circulation, but with positive values over the WNP. This is because this cyclonic system is located on the southern side of a large anticyclonic circulation over northern Asia and the North Pacific (Fig. 7b). As a result, the southern side of the circulation with westward flow dominates southern to eastern China. In contrast, the difference between Periods I and II (Period II minus Period I) shows a southwest–northeast-oriented cyclonic system located east
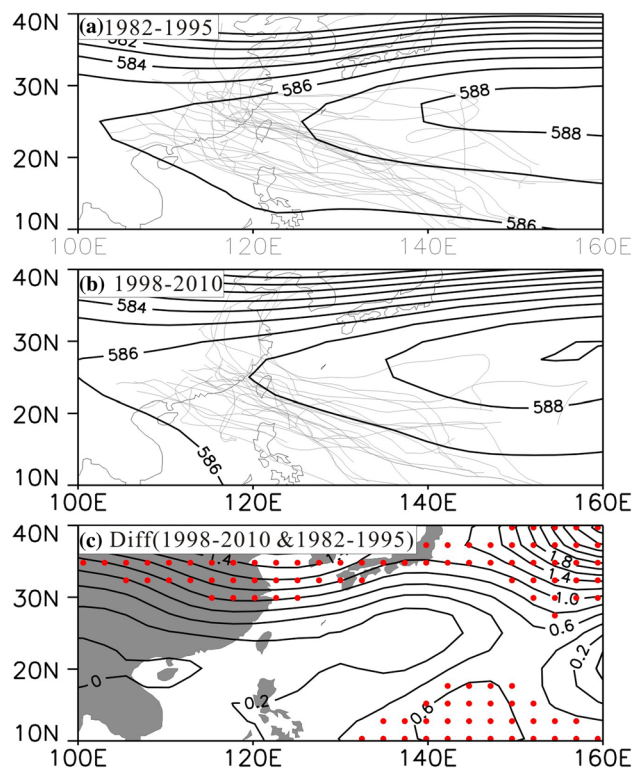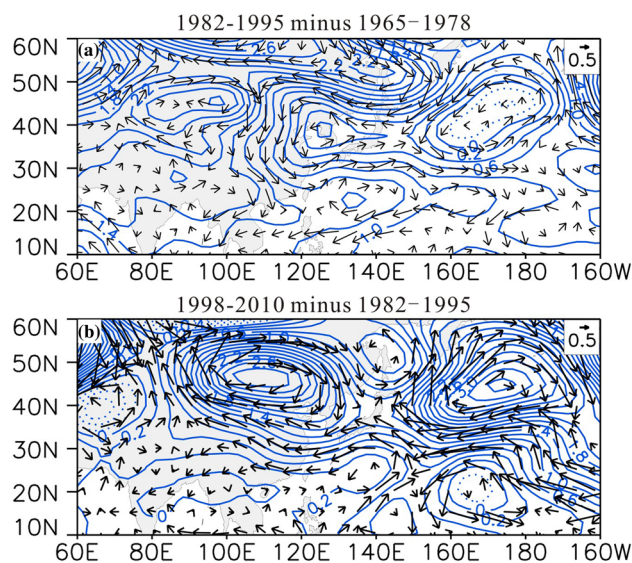
of Japan with two large anticyclonic circulations on either side (Fig. 7a). Eastern China is located at the southern side

of the cyclonic circulation and controlled by westerly flow. The underlying mechanism for the patterns of steering flow during the different Periods is studied in the next section.

4 Effects of PDO phase and tropical IO–WP SST

Tropical SST variability can have a profound impact on the large-scale atmospheric circulation through the atmospheric bridge mechanism (Bjerknes 1966). Therefore, it is vital to explore the relationship between SST variability in the tropical WNP and its adjacent ocean basins with the steering flow over the WNP and the resulting TY landfall on the China coast.

Compared with Period II, warm SST anomalies in the WNP and cool SST anomalies in the eastern subtropical and tropical Pacific can be found during Periods I and III (Fig. 8), which resembles the pattern during a negative PDO phase. Relative to Period II, significant cooling in the tropical IO–WP (10°S–25°N, 50°E–150°E) is found during Period I, but the tropical IO–WP is overall warmer than during Period III (Fig. 8). The 7-year running mean of the IO–WP SST anomalies shows an obvious warming trend since 1965, with a cooling pattern during Period I and warming during Periods II and III (Fig. 9). During the same period, the PDO experienced two phase changes, i.e., a negative phase during Period I, positive phase during Period II, and then another negative phase during Period III (Fig. 9).
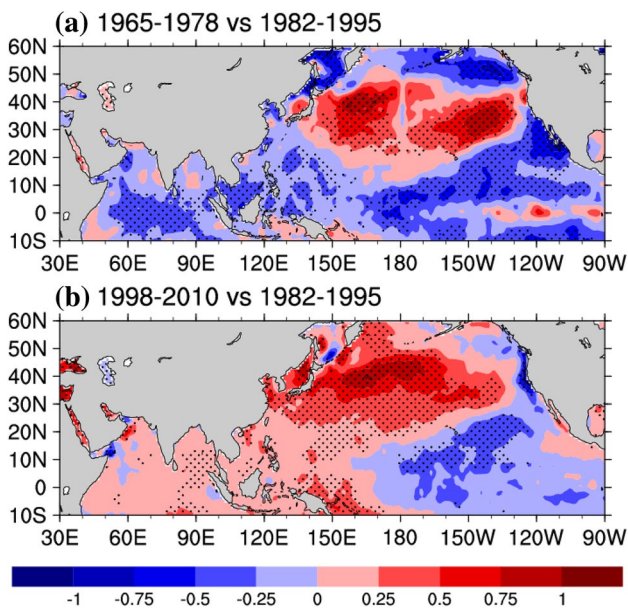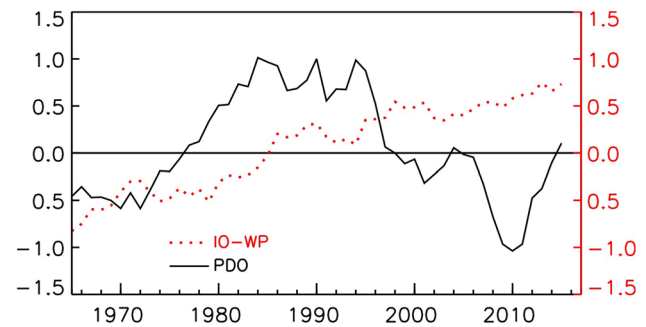
Fig. 9 Time series of 7-year running mean IO–WP (red) and PDO (black) indices during 1960–2015

The 7-year running mean is applied to both the PDO index and SST anomalies during 1960–2015, which gives us confidence in the observed variation during 1965–2010. Based on the time series of the 7-year running average of TY landfall number, PDO index, and SST anomaly index (Figs. 2, 9), we can see that the variation in TY landfall number corresponds well with the PDO phase change, while the tropical IO–WP SST has a positive trend from Period I to Period III. We also find a correlation between the 7-year average PDO index time series, the tropical IO–WP SST anomaly, and TY landfall on the China coast. We find that the correlation coefficient between the PDO index and TY landfall number is 0.71, exceeding the 99% significance level. However, the correlation between the tropical IO–WP SST anomaly and TY landfall is 0.33, only exceeding the 95% significance level. Therefore, we can conclude that the PDO dominates the variation in TY landfall number on the China coast, compared with the tropical IO–WP SST.

The co-influence of the tropical IO–WP SST anomalies and the PDO phase makes it difficult to fully understand the variability of large-scale atmospheric circulation and its resulting TY landfall characteristics. To thoroughly examine the effect of the different PDO phases and tropical IO–WP SST on the large-scale atmospheric circulation anomalies, we regress the PDO index and the detrended IO–WP SST anomalies with the steering flow anomalies during 1965–2010.

The regression of the PDO index with circulations at 500 hPa and steering flow during 1965–2010 shows an anomalous cyclonic center over the WNP, with significantly strong easterly (westerly) flow at the north (south) of the cyclone (Fig. 10a; positive for negative PDO phase and negative for positive PDO phase). This pattern is similar to that in Figs. 3c, 5c, indicting a significant influence of the negative PDO phase on TY landfall on the China coast. The prevailing easterly steering flow can influence the area north of ~ 22°N, possibly leading to TY landfall on the eastern China coast. Over southern China and the SCS, the regression is small and insignificant, indicating a smaller impact of

Fig. 8 Differences in detrended SST between more and fewer TYs making landfall: **a** Period I (1965–1978) minus Period II (1982–1995) and **b** Period III (1998–2010) minus Period II (1982–1995). Dotted areas exceed the 95% significance level
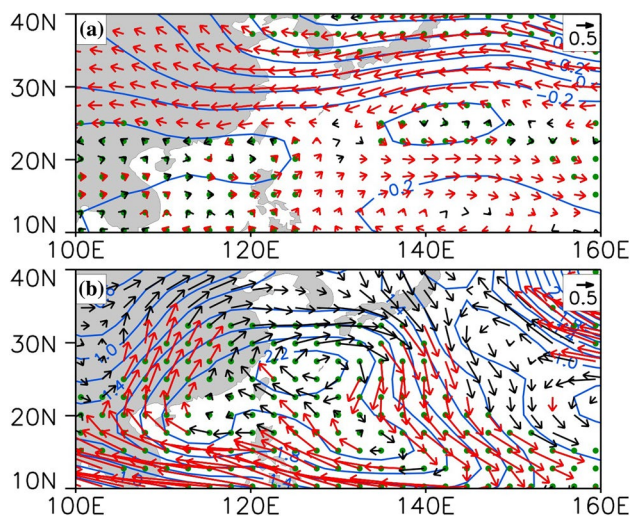
Fig. 10 Regression of **a** PDO index* (−1) and **b** detrended SST anomalies over the tropical IO–WP with steering flow (vector) and 500 hPa geopotential height (contours) anomalies during 1965–2010. Red vectors (green dots) indicate the regression between the PDO index or SST anomalies over the IO–WP with steering flow (500 hPa geopotential height anomaly) exceeds the 95% significance level

Fig. 11 Regression of detrended SST anomalies over the tropical IO–WP with horizontal divergence anomaly at **a** 850 hPa and **b** 200 hPa during 1965–2010. Cross-section of red dots indicates the regression exceeds the 95% significance level

the PDO phase on the TY landfall over the southern China coast.

The regression field of the detrended IO–WP SST anomalies with circulation and steering flow anomalies exhibits an anomalous anticyclonic center over the WNP and the SCS, resulting in strong and prevailing southeasterly flow south of ~25°N east of 140°E, with stronger flow over the southern SCS (Fig. 10b). The warm SST anomaly in the IO can induce a warm Kelvin wave that propagates into the WNP, which intensifies the WPSH (Xie et al. 2009). The warm SST anomalies in the tropical WNP can induce anomalous upward flow, which diverges at the upper layer, flows poleward, and then sinks north of 20°N, which favors more TYs making landfall in the SCS. To further reveal the impact of the tropical IO–WP SST anomalies on the enhanced anomalous anticyclonic circulation, we examine the regression between detrended tropical IO–WP SST anomalies and horizontal divergence at 850 and 200 hPa, respectively. It is found that warm tropical IO–WP SST anomalies can induce divergence (convergence) in the tropical WP at low (high) level, and convergence (divergence) in the subtropical WNP at high (low) level (Fig. 11a, b). Corresponding upward (downward) motion and northerly (southerly) flow at 850 hPa over the tropical WP (subtropical WNP) can be easily seen from the cross-section of JAS meridional and vertical wind anomalies over 110–140°E (Fig. 11c). In addition, the correlation coefficient between the tropical IO–WP SST anomalies and the meridional steering flow anomaly is 0.43, exceeding the 95% significance level. The anomalous southeasterly flow can direct TYs to South and East China,
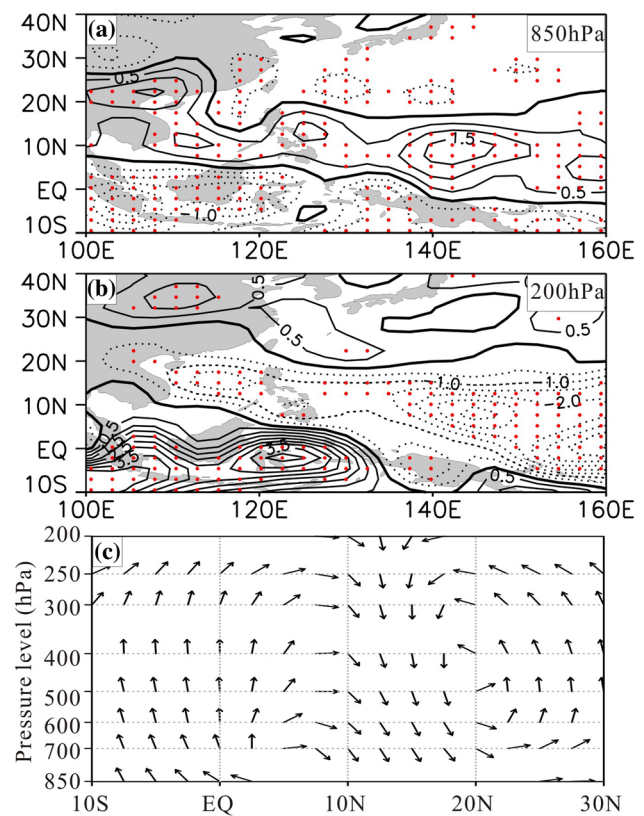
as well as South Asia (Fig. 10b). Both Periods I and III fall within a negative PDO phase, which favors TY landfall on the east China coast; however, the additional tropical IO–WP SST warming during Period III may increase the influence on the atmospheric circulation anomalies, resulting in more TY landfall activity along the South and East China coast (Table 1).

5 Simulated influences of the PDO and IO–WP on steering flows

To further confirm the relationship between the steering flow and the PDO phase and tropical IO–WP SST, we use CAM5 to simulate the atmospheric circulation, with low boundary conditions representing the different PDO phases and IO–WP SST. The model control run is driven by the climatological (1982–2001) monthly SST data from HadISST. The JAS-averaged steering flow from the control run shows a similar pattern to that from the reanalysis data (Figs. 3, 5), exhibiting easterly to southeasterly flow from the WNP to southern China, which turns to westerly flow around 30°N

(Fig. 12a). The simulated geopotential height at 500 hPa also shows a similar pattern to the reanalysis, with an anticyclonic circulation located in the WNP (Fig. 12b). Based on the reasonable simulation of the control run, we are confident to test the sensitivity of several variables on the results. To do this, we design two pairs of sensitivity experiments, based on which we can examine the impact of PDO phase change and IO–WP SST on the steering flow, respectively.

For the first pair of sensitivity experiments, we use a composite of the monthly SST field when the corresponding PDO index is above (below) one standard deviation, and define them as the PDO + (PDO −) scenarios. In the
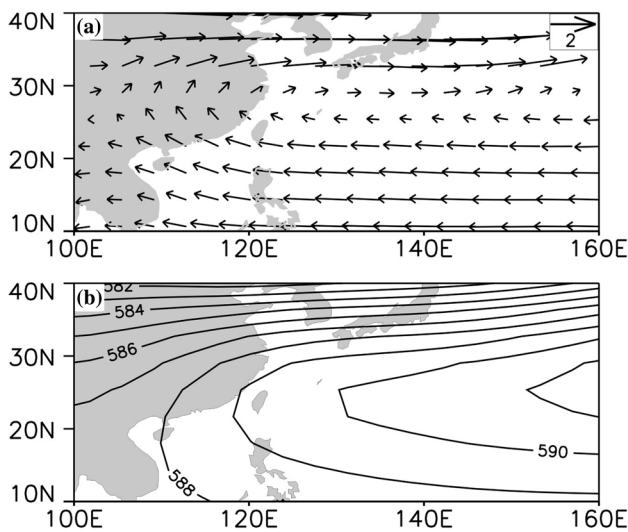

Fig. 12 Model simulated **a** steering flow and **b** 500 hPa geopotential height from the control run

sensitivity run, monthly SST in the original SST dataset is replaced with the PDO + (PDO −) scenarios to drive the model runs, i.e. PDO + (PDO −) runs (Fig. 13a). Each experiment is run for 20 years and the results of monthly ensemble means of the last 10-year runs are analyzed. The difference between the PDO − and PDO + runs shows an easterly steering flow anomaly north of 20°N (Fig. 14a) and a large anomalous cyclonic circulation at the 500 hPa geopotential height over the WNP (Fig. 15a). The pattern closely resembles the regression of the PDO index and steering flow from the reanalysis data. The only difference is that the center of the circulation is located between 20°N, and 25°N, while the simulated center is around 20°N. The anomalous cyclonic circulation at 500 hPa in the WNP suggests that the WPSH is weaker and farther eastward during the negative PDO phase (Liu and Chan 2008).

For the second pair of sensitivity experiments, we use a composite of the monthly SST that is warmer (colder) than one standard deviation over the IO–WP, and define them as the warm (cold) IO–WP scenarios (Fig. 13b). Then, we replace the monthly SST in the original global monthly SST data with the warm (cold) IO–WP scenarios to drive the model runs. Similar to the above PDO runs, these two experiments are also run for 20 years, and the JAS-averaged ensemble mean of the last 10-year runs is used for the further analysis. The difference pattern of steering flow and 500 hPa geopotential height induced by IO–WP warming is very similar to that based on the reanalysis data (Figs. 14b, 15b). Figure 14b shows the difference in steering flow between the warm and cold IO–WP runs. It is found that anomalous easterly flow prevails from 160°E to South Asia and south of 25°N, and anomalous westerly flow prevails from East Asia

Fig. 13 SST difference **a** between PDO + and PDO − scenarios (PDO − minus PDO +) and **b** between warm and cold IO–WP scenarios (warm minus cold)
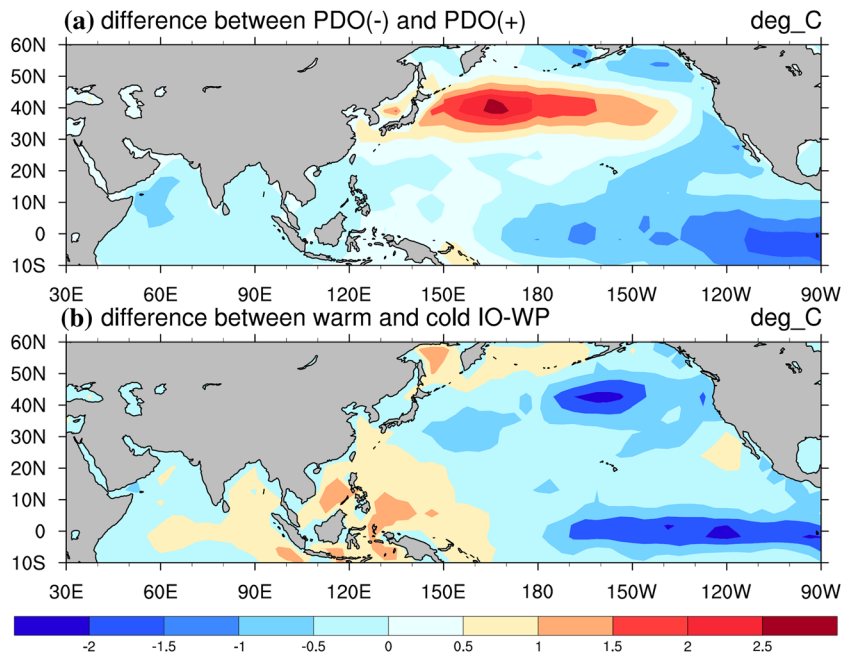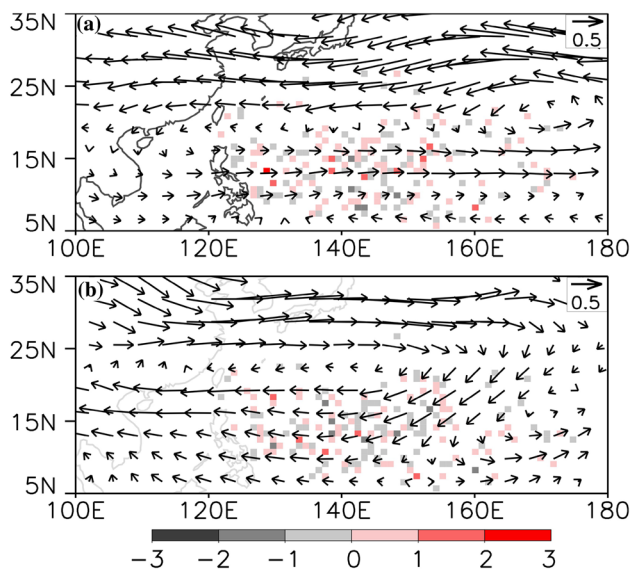
Fig. 14 Steering flow anomaly induced by **a** PDO − and PDO + (PDO − minus PDO +) and **b** warm and cold IO–WP SST (warm minus cold) sensitivity runs. Red shading in **a** and **b** represents the occurrence (over 1 × 1 grid) of TY genesis in the WNP. Red and gray shading in **c** represents the difference (**b** minus **a**)
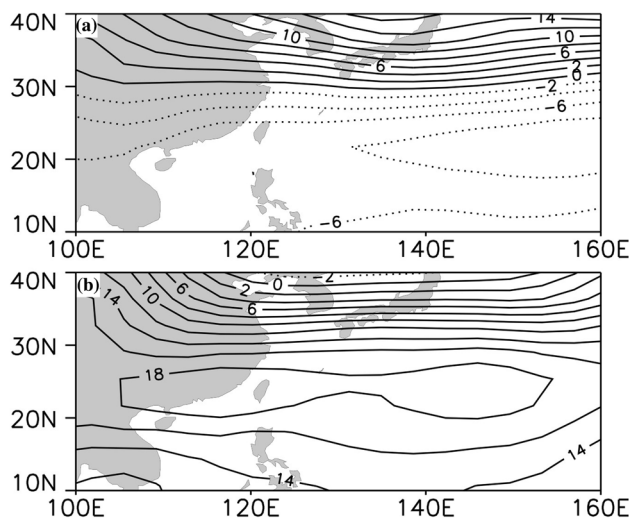

Fig. 15 The 500 hPa geopotential height anomaly induced by **a** PDO − and PDO + (PDO − minus PDO +) and **b** warm and cold IO–WP SST (warm minus cold) sensitivity runs

to the North Pacific, north up to 30°N. Correspondingly, the 500 hPa geopotential height field exhibits an anomalous anticyclonic circulation over the SCS and WNP (Fig. 15b), suggesting that warm IO–WP SST anomalies may result in the westward extension of the WPSH (enhanced subtropical High).

Both the PDO +/PDO − runs and warm/cold IO–WP runs display similar patterns to the reanalysis data. This further

confirms our results that warm tropical IO–WP SST and a negative PDO phase (as occurs during Period III) can lead to overall easterly flow anomalies over East Asia and southeasterly flow over southern Asia, resulting in more TYs making landfall on the China coast.

6 Summary and discussion

The number of TYs making landfall in China has experienced significant interdecadal variation: high (1965–late 1970s); low (early 1980–mid-1990s); and higher (late 1990s–2010). Three typical periods [(I) high (1965–1978); (II) low (1982–1995); and (III) higher (1998–2010)] are chosen to investigate the underlying mechanisms for the interdecadal variation. During a negative PDO phase, the persistent easterly flow anomalies associated with the large-scale circulation over the WNP favors TY landfall on the east China coast. In addition, tropical IO–WP warm SST anomalies can induce the western extension of the WPSH and result in southeasterly flow anomalies in its south, which covers the tropical WNP, the MC, and the SCS. A much higher number of TYs making landfall on the China coast during 1998–2010 may be attributable to the overall SST warming in the tropical IO–WP during a negative PDO phase. Sensitivity experiments with CAM5 further confirm the combined role of the IO–WP SST and negative PDO phase on the steering flow.

Compared with the significant interannual and interdecadal variation in TY landfall numbers, the landfall locations (latitude and longitude) and maximum surface wind show little difference during the three periods. The average landfall latitude during 1965–2010 is 24.8°N, with a slightly more southward location during periods II and III (Fig. 16). The standard deviation of TY landfall latitude shows that TY landfall mainly occurs between ∼ 22°N and 26°N, for all three periods. The average landfall longitude is 116.5°E, with a slight westward shift during Period III, most likely due to more instances of landfall on the southern coast (Fig. 10b). Based on the standard deviation of TY landfall longitude, it is found that TYs make landfall mainly between ∼ 113°E and 119°E for all the Periods. The variation in landfall location, in terms of both longitude and latitude, is relatively larger during Period III. It is also interesting to note that the average maximum surface wind is higher during Period III, while it is relatively lower during Period I. Maximum surface wind during landfall varies from ∼ 18–32 m s⁻¹, with smaller variation during Period II.

The TY landfall along each stretch of the China or Southeast Asia coast exhibits different patterns on various timescales (Huang and Wang 2010; Jin et al. 2013; Liu and Chan 2013). Fully understanding the corresponding mechanisms is very important for TY prediction. In future, climate

Fig. 16 Average landfall latitude, longitude and maximum surface wind speed for WNP TYs in JAS during the different periods (blue for 1965–2010; red for 1965–1978; green for 1982–1995; orange for 1998–2010). Error bars represent one standard deviation of each variable for each period
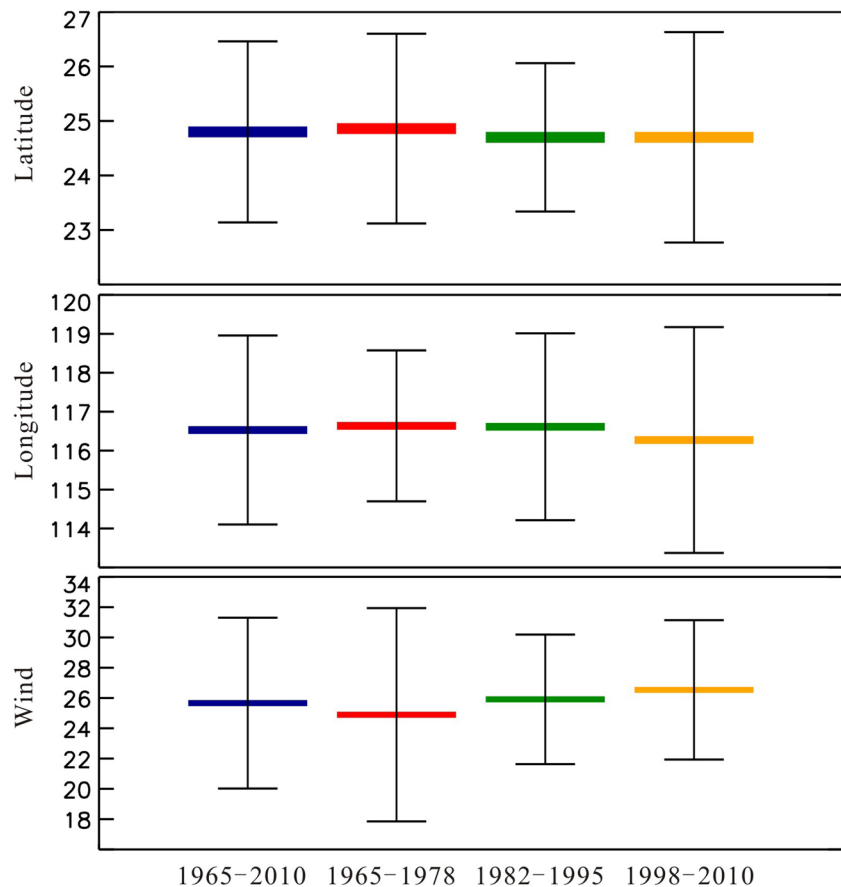
models along with a downscaling method should be used to thoroughly examine the track and landfall characteristics of TYs in the WNP.

References

Bjerknes J (1966) A possible response of the atmospheric Hadley circulation to equatorial anomalies of ocean temperature. Tellus 18:820–829. https://doi.org/10.1111/j.2153-3490.1966.tb00303.x

Bretherton CS, Park S (2009) A new moist turbulence parameterization in the Community Atmosphere Model. J Clim 22:3422–3448

Camargo SJ, Sobel AH (2005) Western North Pacific tropical cyclone intensity and ENSO. J Clim 18:2996–3006

Chan JCL (2006) Comment on "Changes in Tropical Cyclone Number, Duration, and Intensity in a Warming Environment". Science 311(5768):1713b

Chan JCL, Gray AM (1982) Tropical cyclone movement and surrounding flow relationships. Mon Weather Rev 110:1354–1374

Chan JCL, Xu M (2009) Inter-annual and inter-decadal variations of landfalling tropical cyclones in East Asia. Part I: time series analysis. Int J Climatol 29:1285–1293. https://doi.org/10.1002/joc.1782

Chan JCL, Zhou W (2005) PDO, ENSO and the early summer monsoon rainfall over south China. Geophys Res Lett 32:L08810. https://doi.org/10.1029/2004GL022015

Chu PS, Kim JH, Chen Y (2012) Have steering flows in the western North Pacific and the South China Sea changed over the last 50 years? Geophys Res Lett 39:L10704

Dong K, Neumann C (1986) The relationship between tropical cyclone motion and environmental geostrophic flows. Mon Weather Rev 114:115–122

Feng J, Hu D (2014) How much does heat content of the western tropical Pacific Ocean modulate the South China Sea summer monsoon onset in the last four decades? J Geophys Res:Oceans 119(7):4029–4044

Goh A, Chan JCL (2009) Interannual and interdecadal variations of tropical cyclone activity in the South China Sea. Int J Clim. https://doi.org/10.1002/joc.1943

Ho CH, Baik JJ, Kim JH, Gong DY, Sui CH (2004) Interdecadal changes in summertime typhoon tracks. J Clim 17:1767–1776

Holland GJ (1983) Tropical cyclone motion: environmental interaction plus a beta effect. J Atmos Sci 40:328–334

Huang R, Wang L (2010) Interannual variation of the landfalling locations of typhoons in China and its association with the summer East Asia–Pacific pattern teleconnection. Chin J Atmos Sci 34(5):853–864 (Chinese).

Jin CS, Ho CH, Kim JH, Lee DK, Cha DH, Yeh W (2013) Critical role of northern off-equatorial sea surface temperature forcing associated with Central Pacific El Nino in more frequent tropical cyclone movements toward East Asia. J Clim 26(8):2534–2545

Kalnay E, Kanamitsu M, Kistler R et al (1996) The NCEP/NCAR 40-year reanalysis project. Bull Am Meteorol Soc 77:437–470

Kennedy JJ, Rayner NA, Smith RO, Saunby M, Parker DE (2011) Reassessing biases and other uncertainties in sea-surface temperature observations since 1850 part 1: measurement and sampling errors. J Geophys Res 116:D14103

Kim J-S, Kim T, Wang L, Wang X, Moon Y-I (2016) Tropical cyclone activity in the northwestern Pacific associated with decaying Central Pacific El Ninos. Stoch Environ Res Risk Assess 30:1335–1345

Knapp KR, Kruk MC, Levinson DH, Diamond HJ, Neumann CJ (2010) The international best track archive for climate stewardship (IBTrACS). Bull Amer Meteoro Soc 91(3):363–376

Kubota H, Chan JCL (2009) Interdecadal variability of tropical cyclone landfall in the Philippines from 1902 to 2005. Geophys Res Lett 36:L12802

Li G, Chen J, Wang X, Tan Y, Jiang X (2017) Modulation of Pacific Decadal Oscillation on the relationship of El Niño with southern China rainfall during early boreal winter. Atmos Sci Lett 18:336–341. https://doi.org/10.1002/asl.761

Liu KS, Chan JCL (2003) Climatological characteristics and seasonal forecasting of tropical cyclones making landfall along the South China coast. Mon Weather Rev 131:1650–1662

Liu KS, Chan JCL (2008) Interdecadal variability of western North Pacific tropical cyclone tracks. J Clim 21:4464–4476

Liu KS, Chan JCL (2013) Inactive Period of Western North Pacific Tropical Cyclone Activity in 1998–2011. J Clim 26:2614–2630

Neale RB, Richter JH, Conley AJ, Park S, Lauritzen PH, Gettelman A, Williamson DL, Rasch PJ, Vavrus SJ, Taylor MA, Collins WD, Zhang M, Lin S-J (2010) Description of the NCAR Community Atmosphere Model (CAM 4.0). NCAR Tech. Note, NCAR/TN-485+STR, pp 224

Rayner NA, Parker DE, Horton EB, Folland CK, Alexander LV coauthors (2003) Global analyses of sea surface temperature, sea ice, and night marine air temperature, sea ice, and night marine air temperature since the late nineteenth century. J Geophys Res 108:4407. https://doi.org/10.1029/2002JD002670

Saunders MA, Chandler RE, Merchant CJ, Roberts FP (2000) Atlantic hurricanes and NW Pacific typhoons: ENSO spatial impacts on occurrence and landfall. Geophys Res Lett 27(8):1147–1150

Sobel AH, Maloney ED (2000) Effect of ENSO and the MJO on western North Pacific tropical cyclones. Geophy Res Lett 27(12):1739–1742

Wang B, Chan JCL (2002) How strong ENSO events affect tropical storm activity over the western North Pacific. J Clim 15:1643–1658

Wang C, Wang X (2013) Classifying El Niño Modoki I and II by different impacts on rainfall in Southern China and Typhoon Tracks. J Clim 26:1322–1338. https://doi.org/10.1175/JCLI-D-12-00107.1

Wang X, Zhou W, Li C, Wang D (2012) Effects of the East Asian summer monsoon on tropical cyclones genesis over the South China Sea on an interdecadal timescales. Adv Atmos Sci 29:249–262. https://doi.org/10.1007/s00376-011-1080-x

Wang B, Xiang B, Lee J-Y (2013) Subtropical high predictability establishes a promising way for monsoon and tropical storm predictions. Proc Natl Acad Sci USA 110(8):2718–2722. https://doi.org/10.1073/pnas.1214626110

Wang X, Zhou W, Li C, Wang D (2014) Comparison of the impact of two types of El Niño on tropical cyclone genesis over the South China Sea. Int J Climatol 34:2651–2660. https://doi.org/10.1002/joc.3865

Wu L, Wang B, Geng S (2005) Growing typhoon influence on East Asia. Geophys Res Lett 32:L18703. https://doi.org/10.1029/2005GL022937

Xie S-P, Hu K, Hafner J, Tokinaga H, Du Y, Huang G, Sampe T (2009) Indian Ocean capacitor effect on Indo–Western Pacific climate during the summer following El Nino. J Clim 22:730–747

Yang L, Du Y, Wang D, Wang C, Wang X (2015a) Impact of intraseasonal oscillation on the tropical cyclone track in the South China Sea. Clim Dyn 44:1505–1519. https://doi.org/10.1007/s00382-014-2180-y

Yang L, Wang X, Huang K, Wang D (2015b) Anomalous tropical cyclone activity in the northwestern Pacific in August 2014. Bull Amer Meteoro Soc 96:S120-S125. https://doi.org/10.1175/BAMS-D-15-00125.1

Yuan J, Li T, Wang D (2014) Precursor synoptic-scale disturbances associated with tropical cyclogenesis in the South China Sea during 2000-2011. Intl J Climatolo 35(12):3454–3470

Zhang Q, Zhang W, Lu X, Chen Y (2012a) Landfalling tropical cyclones activities in the south China: intensifying or weakening? Int J Climatol 32:1815–1824. https://doi.org/10.1002/joc.2396

Zhang W, Graf HF, Leung Y, Herzog M (2012b) Different El Niño types and tropical cyclone landfall in east Asia. J Clim 25:6510–6523

Zhou W, Li C, Wang X (2007) Possible connection between Pacific Oceanic interdecadal pathway and East Asian winter monsoon. Geophys Res Lett 34:L01701. https://doi.org/10.1029/2006GL027809

Zhou T, Yu R, Zhang J et al (2009) Why the Western Pacific Subtropical High has extended westward since the late 1970s. J Clim 22(8):2199–2215